

Observation of Main-Chamber Heat Loads During Disruptions in DIII-D

E.M. Hollmann,¹ D.S. Gray,¹ N.H. Brooks,² T.E. Evans,² D.A. Humphreys,²
C.J. Lasnier,³ S.C. Luckhardt,¹ A.G. McLean,⁴ R.A. Moyer,¹ D.L. Rudakov,¹
E.J. Strait,² W.P. West,² and D.G. Whyte⁵

¹University of California, San Diego, La Jolla, California, USA

²General Atomics, P.O. Box 85608, San Diego, California 92186-5608, USA

³Lawrence Livermore National Laboratory, Livermore, California, USA

⁴University of Toronto Institute for Aerospace Studies, Toronto, M3H 5T6, Canada

⁵University of Wisconsin, Madison, Wisconsin, USA

One of the most potentially harmful characteristics of tokamak disruptions is the rapid deposition of the initial plasma thermal energy into plasma-facing components. In future large tokamaks, the resulting heat loads can be large enough to cause surface melting or ablation [1]. In diverted tokamaks, the thermal energy is expected to flow into the divertor as a result of fast parallel heat conduction along the scrape-off layer (SOL) into the divertor [2]. Here, it is shown that disruptions in the DIII-D tokamak [3] can result in significant main-chamber heat loads in addition to the expected divertor heat loads. This is done using fast measurements of divertor and main-chamber radiated power. During the initial stage of disruptions where the plasma is hot, main-chamber plasma radiation is expected to result dominantly from main-chamber plasma-wall contact. For the disruptions studied here, we find that roughly 40% of the plasma initial thermal energy is radiated away, implying that roughly 60% is conducted into plasma-facing surfaces. About 80% of the thermal quench radiation comes from the main chamber region. Together, these results suggest that a significant portion of the initial plasma thermal energy, on average, is conducted into the main chamber walls.

The principal diagnostic used here is a fast XUV photodiode array which measures the total plasma brightness along 30 view chords [4]. Because the chords share a single vertex, tomographic inversions cannot be performed on the data; however, the line-integrated brightnesses can give a rough estimate of the spatial distribution of plasma emissivity if assumptions about the emission volumes are made. During disruptions, the XUV array observes a mixing of radiating impurities across the main chamber region on the thermal quench time scale (about 0.5 ms). We assume that the plasma radiation is localized to the plasma edge during the first 0.25 ms of a disruption. After this, plasma radiation is assumed to come from the entire plasma, but is assumed to be poloidally symmetric in the main chamber [5]. These approximations allow a qualitative separation of main-chamber from divertor radiated power. Additionally, an estimate of the total radiated power is obtained. This is found to be relatively insensitive to the exact approximations made about the distribution of emission volumes.

Figure 1(a) shows the energy radiated during the thermal quench (core temperature collapse) of disruptions categorized according to their type: vertical displacement event (VDE), current-limit, density-limit, or beta-limit. On average, it can be seen that roughly 40% (or more) of the initial plasma thermal energy is radiated away. Thus, the thermal energy loss is about half due to conduction and half due to radiation. Figure 1(b) shows the thermal quench main-chamber radiated energy divided by the thermal quench total (main-chamber + divertor) radiated energy. It can be seen that, with very large scatter between cases, about 80% of the thermal quench radiated energy is emitted from the main chamber.

During the thermal quench of disruptions, we expect plasma radiation to be localized dominantly to regions of plasma-wall contact. Volume recombination can be neglected, so the main source of radiating impurities is expected to be carbon sputtered from the graphite wall tiles. This is supported by measurements using a single-chord VUV spectrometer, which show that carbon ions are the dominant source of radiated power during disruptions in DIII-D, typically followed by deuterium, oxygen, and nitrogen. The prevalence of impurity radiation during disruptions has been confirmed using a wavelength-filtered XUV photodiode [6].

Upon being sputtered from the wall, carbon is ionized rapidly past the strongly-radiating low charge states: assuming an ambient plasma with $T_e = 100$ eV and an anomalous radial mixing velocity of 10^5 cm/s, the radiation emission scale length is only of order 10 cm. This localization of plasma emission is supported qualitatively by Fig. 1(b), which shows that disruptions with initial radiation flash in the main chamber (shaded points) tend to have higher thermal quench main-chamber radiated energy fractions.

The correlation between main-chamber radiated power and main-chamber plasma contact can also be demonstrated by looking at Langmuir probe data. This is shown in Fig. 2 for a current-limit disruption. Figure 2(a) shows the main-chamber and divertor radiated power, showing that the divertor radiation increases before the main-chamber radiation does for this disruption. The spikes in main-chamber radiation can be seen to correlate rather well with spikes in the main-chamber Langmuir probe current, Fig 2(b). For these experiments, the

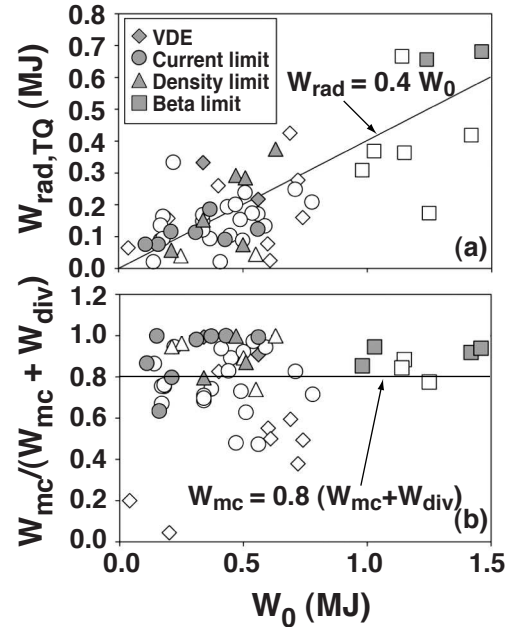


Fig. 1. Fast XUV array measurements of disruptions giving (a) thermal quench radiated energy and (b) thermal quench main-chamber radiated energy fraction as a function of initial stored thermal energy W_0 . Shaded points are disruptions with initial radiation flash in main chamber.

probe was held fixed flush with the port edge to measure the characteristics of plasma striking the outer wall. Probe characteristics show that the large thermal quench spike in ion saturation current corresponds to plasma with $n_e \approx 10^{13} \text{ cm}^{-3}$ and $T_e \approx 100 \text{ eV}$, suggesting that plasma from the vicinity of the separatrix is striking the wall. Figure 2(c) shows C_{III} emission measured with a midplane edge-viewing tangential filterscope. This provides a good diagnostic of main-chamber carbon sputtering and can also be seen to correlate well with

spikes in probe current. Carbon sputtering due to $T_e \approx 100 \text{ eV}$ plasma is roughly consistent with the radiated energy fractions of Fig. 1(a): assuming an incident ion energy of $3T_e$, we obtain an expected ratio of radiated to conducted energy loss of order $Y \times (E_{\text{rad}}/3T_e) \approx 0.13$, where $Y \approx 0.02$ is the D^+ on C sputtering yield and $E_{\text{rad}} \approx 2 \text{ keV}$ is the radiation emitted while fully stripping a carbon neutral.

Among the disruptions studied here, density limit disruptions are most likely to have the initial radiation flash come from the main chamber ($\sim 3/4$ of the time), followed by current limit disruptions ($\sim 1/3$ of the time), beta limit ($\sim 1/4$), and finally VDEs ($\sim 1/5$). The inference is that density limit disruptions are most likely to have conducted heat loads to the main chamber walls. This is not surprising, since the high densities and lower temperatures of plasmas near the density limit imply a lower parallel conductivity, making it easier for cross-field plasma motion to compete with parallel transport into the divertor.

It is well-known that disruptions are associated with large-scale MHD instabilities, and these instabilities appear to be the principal source of the main-chamber heat loads observed here. This can be seen in Fig. 2, where spikes in plasma-wall contact correlate well with spikes in magnetic probe signals, Fig. 2(d). Analysis of magnetic probe signals during the thermal quench in DIII-D indicate that $m=1$ dominates poloidally, with frequent $m=2$ and 3 modes as well, while $n=0$ and $n=1$ dominate toroidally. The $n=0$ motion is inward: this is consistent with the radial force balance shift expected for a rapidly cooling plasma in the (effectively fixed) vertical equilibrium field. The higher-order modes, such as (1/1) and (2/1), often rise too quickly ($< 1 \text{ ms}$) to be tearing modes and might therefore be ideal modes or some coupled combination of ideal and resistive modes. Simulations have shown that a (1/1)

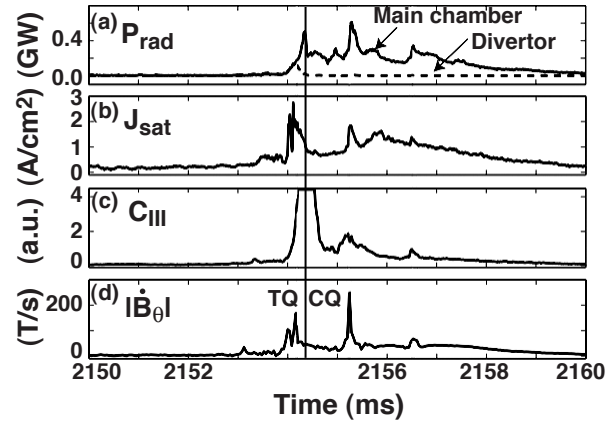


Fig. 2. Time evolution of a current-limit disruption showing (a) radiated power, (b) midplane Langmuir probe current, (c) midplane carbon filterscope brightness, and (d) amplitude of midplane magnetic fluctuations. Vertical line marks end of thermal quench (TQ) and beginning of current quench (CQ).

resistive MHD mode can throw plasma to the wall and can also cause rapid mixing of impurities into the core plasma [7]. A (1/1) kink could be launched during the course of a disruption by main-chamber impurity influx causing a shrinking of the current channel.

In the disruptions studied here, the inward $n=0$ motion often appears to have a slightly larger amplitude than the $n=1$ modes: of the disruptions observed to have an initial radiation flash in the main chamber, about 3/4 had the flash at the inner wall, as opposed to the outer wall. In contrast, a growing $n=1$ mode would be expected to scrape off the separatrix against the outer wall first, because of the slight ballooning nature of the mode shape.

An example of inward $n=0$ motion is shown for a density limit disruption in Fig. 3. Figure 3(a) shows tomographic reconstruction of the soft x-ray emissivity, representing the presence of hot ($T_e > 100$ eV) plasma, while Fig. 2(b) shows reconstruction of the XUV emissivity. At the third time step, hotter plasma strikes the inner wall, Fig. 3(a), and causes a local radiation flash, Fig. 3(b). Magnetic probes indicate that the dominant modes are an inward-moving $(m/n)=(1/0)$ and a smaller $(3/1)$ component.

In conclusion, these radiation measurements and Langmuir probe measurement during disruptions indicate that significant main chamber thermal loads result from large scale MHD activity during the thermal quench of disruptions in DIII-D. These heat loads appear most frequently on the inner wall during density-limit disruptions, but appear to occur to a lesser degree in other types of disruptions and on the outer wall as well. These findings could have important implications for design of main chamber walls in tokamak reactors.

This work was supported by U.S. DOE under DE-FG02-04ER54758, DE-FC02-04ER54698, W-7405-ENG-48, and DE-FG03-96ER54373. Helpful suggestions by Drs. M. Bakhtiari, J.A. Boedo, and R. Pitts are gratefully acknowledged.

- [1] G. Federici, *et al.*, Nucl. Fusion **41**, 1968 (2001).
- [2] I.K. Konkashbaev, Plasma Phys. Report **19**, 496 (1993).
- [3] P. L. Taylor, *et al.*, Phys. Rev. Lett. **76**, 916 (1996).
- [4] D.S. Gray, *et al.*, submitted to Rev. Sci. Instrum. (2004).
- [5] E.M. Hollmann, *et al.*, Phys. Plasmas **10**, 2863 (2003).
- [6] D.S. Gray, *et al.*, Rev. Sci. Instrum. **75**, 376 (2004).
- [6] R.G. Kleva and J.F. Drake, Phys. Fluids B **3**, 372 (1991).

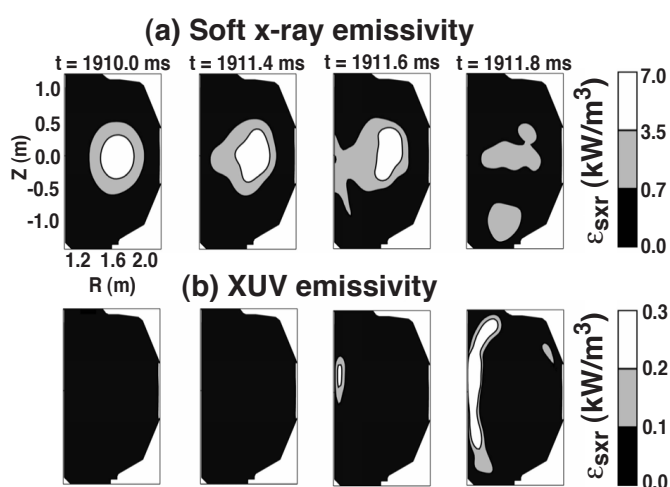


Fig. 3. Time evolution of the thermal quench of a density limit disruption showing (a) soft x-ray emissivity and (b) XUV emissivity.